IEEE Access
Multidisciplinary | Rapid Review | Open Access Journal

Received May 23, 2019, accepted July 4, 2019, date of publication July 10, 2019, date of current version July 25, 2019.

Digital Object Identifier 10.1109/ACCESS.2019.2928146

A Two-Dimensional Frequency Modulation Deception Jamming Against ISAR

NING TAI[1,2], HUAN LIN[2], YONGWEI LU[2], HUI HAN[1], XIONG XU[1], AND YONGHU ZENG[1]

[1]State Key Laboratory of Complex Electromagnetic Environment Effects on Electronics and Information System, Luoyang 471003, China
[2]Luoyang Electronic Equipment Test Center, Luoyang 471000, China

Corresponding author: Ning Tai (358041578@qq.com)

ABSTRACT This paper proposes a false target jamming method for countering ISAR based on two-dimensional frequency modulation. The target template is created according to the ISAR image of a true target. Then the range modulation signal, of which the frequency relates to each range cell of the template, is generated using direct digital synthesizer. The creation of modulation signal can be implemented parallel to accelerate the algorithm. All the range modulation signals are added up after amplitude adjustment and Doppler phase modulation. At last the jamming signal is derived from the multiplication between the intercepted radar signal and the modulation signal. Using the property of linear frequency modulated signal and frequency modulation, the jamming signal creates a false target of high fidelity after ISAR imaging. The proposed method is real-time when producing a false target with simple structure. For a template consists of a great many scatterers, the jamming algorithm is separated into real-time stage and off-line stage, which fulfills the generation of modulation signal after obtaining the radar parameters. The jamming effect on ISAR is presented through simulation results and the validity of the method is verified.

INDEX TERMS Frequency modulation, deception jamming, DDS, ISAR, LFM.

I. INTRODUCTION

Inverse synthetic aperture radar (ISAR) has the ability to provide two-dimensional (2-D) images of the observation target. Due to the all-weather, day-and-night, and high resolution property, ISAR has been widely applied in both civil and military fields [1]–[3]. Along with the development of ISAR technology, various electronic countermeasures have been proposed against this powerful imaging radar to prevent it from detecting or imaging the potential target [4], [5]. The jamming approaches can be classified into two categories according to the energy source: passive jamming and active jamming [6]–[8].

The passive jamming does not emit electromagnetic signals, but utilizes rotating object [9], or makes use of special materials to change the reflection property of the target [10], [11]. Covered by a cross-shaped metamaterial, the target turns into two false targets on the ISAR image and none of the targets is located at the real position [12]. The phase-switched screen (PSS) imposes phase modulation onto the radar signal to redistribute the energy of signal into sidebands [13]. If the radar signal is a wideband linear frequency modulated (LFM) signal, the signal reflected by PSS may still occupy some bandwidth of the radar receiver, which induces multiple false targets according to the PSS property [14], [15]. Active frequency selective surface (AFSS) can dynamically switch its scattering intensity and impose amplitude modulation onto the radar signal [16]. This method can be treated as the passive implementation of the interrupted-sampling repeater jamming, capable of generating 3-5 false targets along the range or azimuth direction.

In general, the property of passive jamming is fixed since it relies on the physical characteristic of the material. The active jamming is more flexible because the jamming signal is transmitted by a jammer, which can set the jamming parameters dynamically. The active jamming can be classified into barrage jamming and deception jamming. A barrage jammer transmits noise-like signals with large power, aiming at covering the echo of real target. Considering that ISAR achieves a high signal-to-noise ratio (SNR) by coherent processing both along the two dimensions, the power of jammer must be very large to guarantee the valid jamming [17]. Thus more

The associate editor coordinating the review of this manuscript and approving it for publication was Ravibabu Mulaveesala.

attentions have been paid to the deception jamming method, which simulates the true target echo and achieves part of the processing gain [18], [19].

How to modulate the movement property, the structure information, and the scattering property of a target onto the intercepted radar signal is an important problem to deception jammer. The modulation method directly determines the fidelity of the false target and the jamming effect. Various methods, such as scatter-wave jamming [20]–[22], digital image synthesizer (DIS) method [23], [24], and convolution method [25], are proposed to deal with this problem. The scatter-wave method transmits the jamming signal to the protected target instead of the radar. After reflected by the target, the jamming signal contains all the target's information, which makes the jamming signal similar to the true target echo. Based on the model of scatter-wave jamming, the sub-Nyquist jamming [26], the 0-π phase modulation method [27]–[29], and the micro-motion jamming method [30], are developed and analyzed. Nevertheless, the application of scatter-wave method is quite difficulty because the jammer's receiving antenna must head to ISAR and the transmitting antenna should point to the real target. Meanwhile, the power of the jamming signal is hard to satisfy the demand for a successful jamming.

The DIS method, a milestone countermeasure, can form a false target as same as the target template on the ISAR image. But this method suffers heavy computation load, lacks of vivid target template, and is hard to simulate the scattering property of the target. This shortcoming is overcome by the convolution method where the electromagnetic scattering model is used to represent a target. But the convolution method also requires large computation sources and it is very time-consuming when the template is quite large. Considering the status of ISAR deception jamming, we propose a real-time jamming algorithm against ISAR based on 2-D frequency modulation. The target template is created from a real ISAR image to guarantee the fidelity. The algorithm is real-time when creating a small false target. It can be separated into off-line stage and real-time stage when the computation resource is limited. Only one multiplication is needed to generate the jamming signal in the real-time stage.

II. THE PROPOSED JAMMING METHOD

A. PROPERTY OF THE TARGET ECHO

To begin with, we analyze the property of radar signal reflected by a target. In Fig. 1, the *xoy* coordinate system is established on the center of jammer as the original point o. The y-axis, of which the positive direction is defined as the range direction, stands for the light-of-sight (LOS) of ISAR. The x-axis is perpendicular to the y-axis and its positive direction is named as the azimuth direction. The ISAR locates at position I in this figure.

We use point A in the target to analyze the property of target echo. The radar wave reflected by A is the delayed replica of the transmitted signal after time delay $2|IA|/c$,

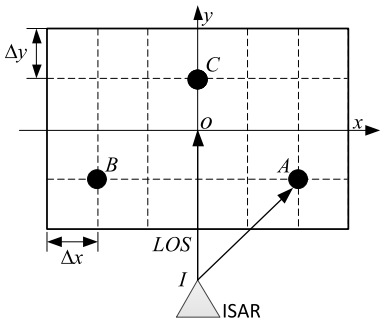

FIGURE 1. The model of ISAR imaging.

where c denotes the speed of electromagnetic wave, $|IA|$ is the instantaneous distance from ISAR to point A. After the translational motion is compensated, the movement of target can be treated as the rotating model. Suppose that the coordinate of point A is (x_A, y_A) and point A is rotating with the target at an angular velocity ω, then the coordinate of A at time t is:

$$\begin{aligned} x_A &= r\cos(\theta_0 + \omega t) \\ y_A &= r\sin(\theta_0 + \omega t) \end{aligned} \tag{1}$$

where r is the slant distance from point A to origin o. θ_0 is the included angle between point A and the positive direction of x-axis at initial time.

Suppose that ISAR locates at $(0, -r_0)$, then the instantaneous distance from point A to ISAR is:

$$|IA| = \sqrt{x_A^2 + (y_A + r_0)^2} \approx r_0 + r\sin(\theta_0 + \omega t) = r_0 + y_A \tag{2}$$

Equation (2) is obtained in the far field where $r_0 \gg r$. $|IA|$ can be approximated as the sum of r_0 and the y-coordinate of point A.

The corresponding Doppler frequency of point A is:

$$f_d(A) = \frac{2}{\lambda}\frac{d|IA|}{dt} = \frac{2\omega r\cos(\theta_0 + \omega t)}{\lambda} = \frac{2\omega}{\lambda}x_A \tag{3}$$

where λ is the wavelength of radar signal.

From (3) we see that the Doppler frequency relates to the angular velocity ω, the wavelength λ and the x-coordinate of point A. Because the range processing is independent from the azimuth processing in ISAR imaging, we can build up the range modulation signal and the azimuth modulation signal, respectively.

B. RANGE MODULATION SIGNAL

We select an ISAR image of a target as the template, of which the size is $M\Delta y$ (in range) $\times$ $N\Delta x$ (in azimuth). M and N are the numbers of template cells in range direction and azimuth direction, respectively. Δy and Δx mean the resolution of range direction and azimuth direction, respectively. According to the time-frequency property of LFM signal, the matched filter result of the LFM signal with certain frequency modulation will deviate from its original location [15]. In this paper, the central point of false target is at the jammer's location. Then the relative distance of each scatterer

on the false target is computed by taking the origin o as a reference. In terms of point A, the relative distance between origin o and A is approximately equal to y_A, so the frequency of range modulation signal is:

$$f_m(A) = \frac{2\gamma y_A}{c} \tag{4}$$

where γ is the chirp rate of LFM signal.

From (4) we see that the frequency is directly proportional to γ and y_A. In the same way, the modulation signal corresponds to each range cell of the target template can be descried as:

$$I_{rm}(t) = \exp(j2\pi \frac{2\gamma m\Delta y}{c} t) = \exp(j2\pi f_m t) \tag{5}$$

where t is the fast-time. m stands for the m_{th} range cell of the target template.

C. AZIMUTH MODULATION SIGNAL

In Fig. 1, some scatterers may locate at different azimuth cells but share with the same range cell. ISAR distinguishes these scatterers by their Doppler frequencies. So we need modulate different Doppler frequencies onto the range modulation signal according to the azimuth location of each scatterer. The azimuth modulation signal is:

$$I'_{rm}(t, t_a) = \exp(j2\pi f_m t) \times \exp(j2\pi f_{dn} t_a) \tag{6}$$

where f_{dn} is the Doppler frequency of each scatterer. t_a is the slow-time. The expression of Doppler frequency is:

$$f_{dn} = \frac{n\Delta x \times \mathrm{PRF}}{N_d \delta_a} \tag{7}$$

where n is the n_{th} azimuth cell of the target template. N_d is the number of radar pulses used for an ISAR image. δ_a is the azimuth resolution of ISAR image. PRF stands for the pulse repetition frequency of the radar signal.

The second exponential term in (6) only varies with the slow-time t_a, which means that it remains unchanged during the pulse width of radar signal. It attaches an initial phase to the range modulation signal.

The azimuth resolution of ISAR image is [3]:

$$\delta_a = \frac{\lambda \times \mathrm{PRF}}{2\omega N_d} \tag{8}$$

Substituting (8) into (7), we derive:

$$f_{dn} = \frac{2\omega n\Delta x}{\lambda} = \frac{2\omega}{\lambda} x \tag{9}$$

Equation (9) indicates that the Doppler frequency of each scatterer relates to the x-coordinate of the scatterer, the wavelength λ, and the rotating angular velocity ω. ω and the scatterer's coordinate are controlled by the jammer.

Now we can get the azimuth modulation signal for each scatterer. In order to create a modulation signal which is able to reflect the scattering coefficients of different scatterers, the modulation signal should be modified by introducing the scattering coefficient σ.

$$I'_{rm}(t, t_a) = \sigma \times \exp(j2\pi f_m t) \times \exp(j2\pi f_{dn} t_a) \tag{10}$$

In the real scene, the target echo is the superposition of radar signal reflected by each scatterer (in different range cells, different azimuth cells) in space. So we sum all the azimuth modulation signals which locate at the same range cell. Then (10) turns into:

$$I_m(t, t_a) = \sum_{n=1}^{N} \sigma(m, n) \times \exp(j2\pi f_m t) \times \exp(j2\pi f_{dn} t_a) \tag{11}$$

Due to the time-frequency coupling property of LFM signal and the linearity of matched filter process, the modulation signal of each range cell can be summed to derive one modulation signal.

$$I(t, t_a) = \sum_{m=1}^{M} \sum_{n=1}^{N} \sigma(m, n) \times \exp(j2\pi f_m t) \times \exp(j2\pi f_{dn} t_a) \tag{12}$$

Equation (12) indicates that the final modulation signal is the weighted superposition of multiple single-tone signals, which can be produced by direct digital synthesizer (DDS). The time length of $I(t, t_a)$ is determined by the fast-time t, which is usually equal to the pulse width of radar signal.

D. THE JAMMING SIGNAL

Suppose that ISAR transmits an LFM signal and its expression in base band is:

$$s(t) = \mathrm{rect}(\frac{t}{T_p}) \times \exp(j\pi\gamma t^2) \tag{13}$$

where T_p, γ is the pulse width and the chirp rate, respectively. The bandwidth of LFM signal is $B = \gamma T_p$.

The jamming signal is the multiplication result of $s(t)$ and the modulation signal $I(t, t_a)$. Without loss of generality, we still use point A, of which the scattering coefficient is set to 1, to discuss the jamming signal, which is:

$$\begin{aligned} s_{jA}(t, t_a) = {} & \mathrm{rect}(\frac{t}{T_p}) \times \exp(j\pi\gamma t^2) \\ & \times \exp(j2\pi \frac{2\gamma y_A}{c} t) \times \exp(j2\pi \frac{2\omega x_A}{\lambda} t_a) \end{aligned} \tag{14}$$

From (14) we know that the jamming signal changes with the slow-time t_a due to the third exponential terms, which refers to the Doppler frequency.

Now we obtain the expression of the jamming signal. To sum up, the jamming algorithm includes the generation of the modulation signal and the creation of the jamming signal. The procedure to create the modulation signal is shown in Fig. 2(a). Because the frequency in (5) or (9) is constant for each cell of the target model, the modulation signal corresponds to the range or azimuth cell can be computed parallel to enhance the real-time performance of the jamming algorithm. The amplitude modulation and the summation of all the modulation signals are implemented by multiplications and additions using pipeline technology. The procedure to generate the modulation signal is listed as follows:

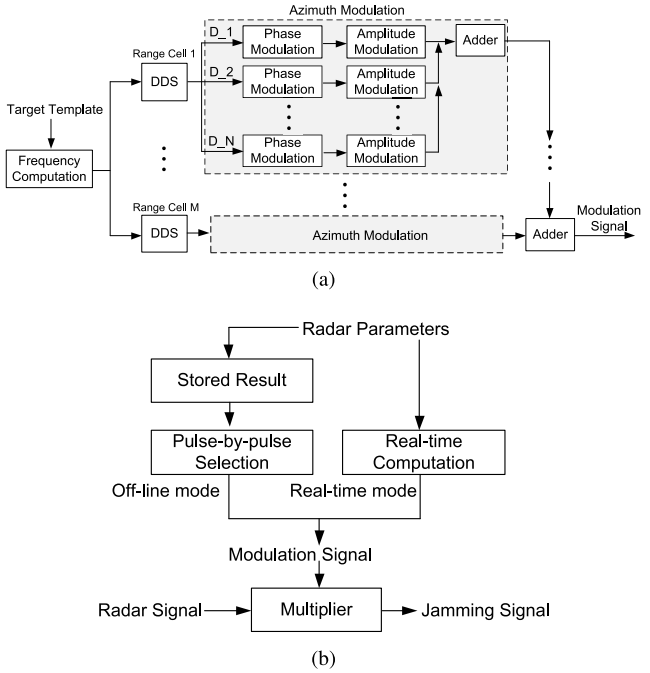

FIGURE 2. Block diagram of the 2-D frequency modulation jamming algorithm. (a)The generation of the modulation signal. (b)The creation of the jamming signal.

1) Create range modulation signal using DDS.
2) Modulate Doppler phase onto each range modulation signal.
3) Conduct amplitude modulation on each range modulation signal.
4) Sum all the range modulation signals to obtain the final modulation signal.

We see that the modulation signal is obtained after 4 steps. Since DDS outputs signal consecutively after the frequency value is set, the Doppler phase can be added to the DDS output signal by complex multiplication or phase rotation. Then the phase-modulated signal is multiplied by the scattering coefficient of each scatterer. At last, the modulation signal corresponding to each range cell is summed to derive one modulation signal. Because only additions and multiplications are included in the above steps, these procedures can be implemented by pipeline technology to consecutively generate the modulation signal. Taking the processing time of FPGA into consideration, the modulation signal starts to output data after several periods of FPGA clock, i.e., tens or hundreds of nanoseconds. Thus the proposed algorithm is real-time because only one time of multiplication between the modulation signal and the intercepted radar signal is needed to produce the jamming signal.

Since the creation of each range modulation signal is implemented parallel to accelerate the algorithm, the consumption of computation resource increases when the scatterers of target model become more. If the target consists of fewer (tens or hundreds of) scatterers, the computation resource of FPGA is enough. When the target is complex in structure and has thousands of scatterers, the generation of the modulation signal can be realized in off-line since only a few radar parameters are needed, as shown in Fig. 2(b). On the off-line occasion, the real-time performance of the method degenerates because the jamming signal cannot be produced during the time when jammer creates the modulation signal.

III. ISAR IMAGING FORMATION

A. 1-D RANGE PROFILE

According to [7], the matched filter result of the LFM signal with frequency shift f_r can be written as (the phase item is omitted):

$$P_0(t) = \left(1 - \frac{|f_r|}{B}\right) \times \mathrm{sinc}\left(B\left(t + \frac{f_r}{\gamma}\right)\right) \tag{15}$$

where

$$\mathrm{sinc}(x) = \frac{\sin(\pi x)}{\pi x} \tag{16}$$

From (15) we see that when $f_r \neq 0$, $P_0(t)$ peaks at $t = -f_r/\gamma$. Let's analyze the matched filter result of the jamming signal in (14). The 1-D range profile of the jamming signal is:

$$I_1(t, t_a) = \left(1 - \frac{|2\gamma y_A/c|}{B}\right) \times \mathrm{sinc}\left(B\left(t + \frac{2y_A}{c}\right)\right) \times \exp(j2\pi \frac{2\omega x_A}{\lambda} t_a) \tag{17}$$

The maximal value of (17) appears at $t_A = -2y_A/c$. Converting t_A from time-domain to range-domain, the result stands for a distance which equals to the y-coordinate of point A. The negative sign '-' indicates that the range position of A on ISAR image is opposite to its coordinate in target template.

B. 2-D ISAR IMAGE

In general, ISAR achieves the high resolution along the azimuth direction by conducting fast Fourier transform (FFT) in the slow-time domain. Carrying out FFT of (17) in slow-time domain, the false target on the range-Doppler plane has an expression as:

$$I_2(t, f) = T_M \left(1 - \frac{|2\gamma y_A/c|}{B}\right) \times \mathrm{sinc}\left(B\left(t + \frac{2y_A}{c}\right)\right) \times \mathrm{sinc}\left(T_M\left(f - \frac{2\omega}{\lambda} x_A\right)\right) \tag{18}$$

where T_M is the processing time for an ISAR imaging.

In (18), the peak value along the azimuth direction appears at:

$$f_A = \frac{2\omega}{\lambda} x_A \tag{19}$$

The corresponding azimuth location of f_A on the ISAR image is:

$$x = \frac{f_A}{\mathrm{PRF}/N_d} \times \delta_a = x_A \tag{20}$$

Equation (20) shows that the x-coordinate of point A can be correctly formed by ISAR after the azimuth processing.

Previous analysis validates that the 2-D frequency modulation jamming signal is valid to generate a false point on the ISAR image. Considering the linearity of frequency modulation, LFM signal, and ISAR imaging processing, the proposed method is effective to generate a false target on ISAR image.

IV. PARAMETERS DISCUSSION

A. ESTIMATING ERROR OF CHIRP RATE

According to (5), the range size of false target is contained in the frequency of modulation signal, which is based on the estimating value of chirp rate γ. In consideration of the estimating error in γ, the frequency of range modulation signal should be written as:

$$f'_m = \frac{2\gamma' y}{c} \tag{21}$$

where γ' is the estimating value and y is the y-coordinate of the false target.

Since the deviated range distance of the matched filter result relates to the modulation frequency, the corresponding range size of (21) is:

$$y' = \frac{\gamma'}{\gamma} y = (1 + \eta_r) y \tag{22}$$

where

$$\eta_r = \frac{\gamma' - \gamma}{\gamma} \tag{23}$$

is the estimating error of γ.

Equation (23) illuminates that the range size of the false target is affected by η_r. The false target's length on the ISAR image may be larger or smaller than its true size due to relationship between γ and γ'.

B. ESTIMATING ERROR OF WAVELENGTH

According to (9), the Doppler frequency of each scatterer relates to ω and λ. Now we use λ' to represent the estimating value, then the Doppler frequency in (9) turns into:

$$f'_{dn} = \frac{2\omega}{\lambda'} x \tag{24}$$

After ISAR processing, the x-coordinate of false target corresponds to (24) is:

$$x' = \frac{\lambda}{\lambda'} x = (1 + \eta_\lambda) x \tag{25}$$

where η_λ is defined as the estimating error of λ.

$$\eta_\lambda = \frac{\lambda - \lambda'}{\lambda'} \tag{26}$$

when $\lambda' > \lambda$, the Doppler frequency is smaller than we need, which causes the azimuth size of the false target to decrease. On contrary, the false target becomes larger along the azimuth direction.

C. THE INFLUENCE OF ROTATING ANGULAR VELOCITY

According to (8), the azimuth resolution of an ISAR image is determined by the rotating angular velocity ω of the target, which is an estimating value to ISAR. In this paper, ω is set by the jammer, so the estimating value ω' in ISAR maybe different from the jamming parameter ω.

After introducing ω', the azimuth size of target is:

$$x' = \frac{\omega}{\omega'} x = (1 + \eta_\omega) x \tag{27}$$

where

$$\eta_\omega = \frac{\omega - \omega'}{\omega'} \tag{28}$$

is defined as the estimating error of ω.

Because the estimating error in ω' affects the azimuth resolution of ISAR image, the azimuth size of the false target will be larger than its real size when $\omega' < \omega$, whereas it will be smaller.

D. AMPLITUDE COMPENSATION

According to (15), the amplitude of $P_0(t)$ decreases when $f_r \neq 0$. After frequency modulation, the frequency span of the modulated signal will exceed the bandwidth of LFM signal and the exceeded part cannot achieve the processing gain. Considering a scatterer located far from the origin, the amplitude of the signal which represents for the scatterer decreases heavily due to the large frequency shift. To guarantee that the amplitude of each scatterer coincides with the target template after ISAR imaging, an amplitude compensation coefficient for each range cell is needed.

$$A_r = \frac{B}{B - |f_r|} \tag{29}$$

By introducing A_r, the modulation signal of each range cell has different amplitude gains to compensate the amplitude loss brought by the frequency shift.

E. FREQUENCY MODULATION RESOLUTION

In this paper, the range modulation signal consists of multiple single-tone signals, each of them represents one range cell of the target template. To distinguish two neighboring scatterers, the frequency resolution of range modulation signal is:

$$f_{ro} = \frac{2\gamma \Delta y}{c} \tag{30}$$

which is the demand for minimal frequency of DDS. Since f_{ro} is directly proportional to Δy and γ, the jammer can set the resolution of DDS according to the template's resolution and the typical value of γ.

From Fig. 3(a) we see that when B is fixed, the frequency value decreases as the pulse width increases. When B becomes large, the frequency value increases since $\gamma = B/T_p$. To output a signal of lower frequency, the bit width of the phase-adder in DDS must increase and it consumes more resources. Generally speaking, the bandwidth of LFM signal is quite large in ISAR imaging, so the frequency

TABLE 1. Comparison of the computational complexity.

	Procedure	Number of multiplications	Number of additions
T-DIS	2-D FFT	$M_d \times M_r \log_2 M_r + M_r \times M_d \log_2 M_d$	$M_d \times (M_r \log_2 M_r)/2 + M_r \times (M_d \log_2 M_d)/2$
	Correction matrix	$M_r \times M_d$	$2 \times M_r \times M_d$
	Linear interpolation	$2 \times M_r \times M_d \times 2$	$3 \times M_r \times M_d \times 2$
	Jamming modulation	$M_s \times N_d$	0
2-D FMDJ	DDS	0	$M \times M_s \times N_d + N \times N_d$
	Doppler modulation	0	$K \times M_s \times N_d$
	Amplitude modulation	$K \times M_s \times N_d$	0
	Summation	0	$(K-1) \times M_s \times N_d$
	Jamming modulation	$M_s \times N_d$	0

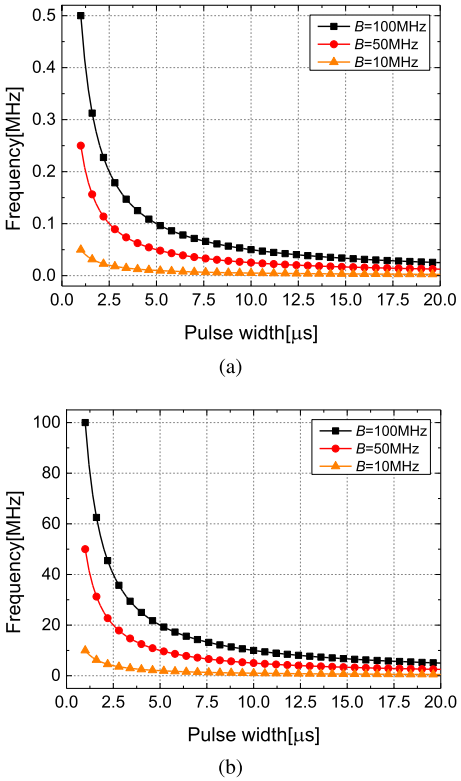

FIGURE 3. The frequency resolution and the maximal frequency value of DDS. (a)The demand for frequency resolution. (b)The maximal frequency value.

resolution for a template with 0.75m range resolution varies from 25-500kHz when $B = 100$MHz, which is appropriate for DDS.

The maximal output frequency of DDS is determined by the range size of target template. The frequency in Fig. 3(b) refers to a target of 150m in length. Considering the amplitude loss of the LFM signal with frequency modulation after matched filter, the maximal frequency should better be less than $B/2$.

$$\frac{2L\gamma}{c} \leq \frac{B}{2} \tag{31}$$

where L denotes the range size of the target template. Substituting $\gamma = B/T_p$ into (31), we arrive at:

$$T_p \geq \frac{4L}{c} \tag{32}$$

For example, the jamming method performs well to generate a target of 150m on ISAR image if the pulse width of LFM signal is larger than 2μs, which is easily satisfied for most ISAR signals.

F. COMPUTATION RESOURCE REQUIREMENT

The comparison of the computational complexity between the proposed two-dimensional frequency modulation deception jamming (2-D FMDJ) method and T-DIS method [31] is presented in Table. 1. Since the computational complexity relates to the samples number of the intercepted radar signal, we assume that the samples number is M_s for one radar pulse and the ISAR image is formed by N_d pulses. The target template consists of $M \times N$ cells.

In T-DIS method, the generation of the modulation signal begins from the 2-D FFT. The FFT number is M_r and M_d for range direction and azimuth direction, respectively. M_r ($M_r > M_s$) or M_d ($M_d > N_d$) is a power of two for the fast computation. For an FFT of M_r points, the number of multiplications is $M_r \log_2 M_r$ and the number of additions is $\frac{M_r}{2} \log_2 M_r$. Then the total number of multiplications for the 2-D FFT is $M_d \times M_r \log_2 M_r + M_r \times M_d \log_2 M_d$. The total number of additions is $\frac{M_d}{2} \times (M_r \log_2 M_r) + \frac{M_r}{2} \times (M_d \log_2 M_d)$. The T-DIS method requires a correction matrix to modify the modulation signal. The number of multiplications for the correction matrix is $M_r \times M_d$. Next the modulation signal is re-sampled using linear interpolation. One time of linear interpolation calls for 3 additions and 2 multiplications. Thus the computation of 2-D linear interpolation requires $2 \times M_r \times M_d \times 2$ multiplications and $3 \times M_r \times M_d \times 2$ additions. At last, to produce the jamming signal, the modulation signal is multiplied by the radar signal pulse-by-pulse, which demands $M_s \times N_d$ times of multiplications and the redundant data of the modulation signal is not used.

In our method, the first step is to generate the range modulation signal using DDS [33]. After the parameters of radar signal are estimated, the frequency of the range modulation signal or azimuth modulation signal only relates to the coordinate of each scatterer. Since the coordinate of each scatterer and the target model are known to the jammer, the modulation signal corresponds to each scatterer can be generated at the same time, i.e., the creation of modulation signal can be implemented parallel. Then all the modulation signals after Doppler phase modulations are summed to derive one modulation signal by additions using pipeline technology. Since DDS synthesizes a signal based on phase accumulation, only additions are required. In table. 1, K refers to the scatterers number of the false target. Firstly, DDS outputs M number of range modulation signals using $M \times M_s \times N_d$ additions. The Doppler phase created by DDS requires $N \times N_d$ additions. Then the Doppler phase modulation onto the range modulation signals corresponding to all the scatterers needs $K \times M_s \times N_d$ additions. The amplitude modulation calls for $K \times M_s \times N_d$ multiplications. $(K-1) \times M_s \times N_d$ additions are used to sum all the modulation signals. At last, the jamming signal is obtained by $M_s \times N_d$ multiplications.

We present the ratio of computation complexity of our method to T-DIS method in Fig. 4. When M_s, M_r, M_d and N_d are set, the number of multiplications or additions in T-DIS method is fixed, while the computation times of our method change as the scatterers number K. We see that as K increases, our method requires more computations. In our method, the modulation signal corresponds to each scatterer must be computed at each radar pulse and this makes the proposed method work in real-time. From Fig. 4 we think the increasing computation load is acceptable.

Next we analyze the real-time performance of the two methods. The most time consuming procedure of T-DIS method is the 2-D FFT, of which the calculation delay depends on the FFT numbers. Furthermore, according to Xilinx FPGA, the maximal number of FFT IP core is 65536. If the sample numbers of the intercepted radar signal are larger than 65536, the user has to develop the FFT algorithm by himself. Generally speaking, the bandwidth of ISAR signal is very large and the pulse width of ISAR signal is quite long. For example, suppose that the bandwidth of ISAR is 500MHz, the pulse width is 100μs, and the pulses number for an image is 256, then the samples number should be $500 \times 100 \times 2 = 100000$ when Nyquist sampling theorem is satisfied. The computation delay of FFT is 100000 clock periods, which equals to 200μs when FPGA operates at a clock of 500MHz. Considering the computation resource of FPGA, N (N refers to the number of azimuth cells in the target template) times of FFT along the range direction can be implemented at the same time. But the FFT along the azimuth direction must be implemented serially because 100000 times of FFT working parallel is impossible for FPGA. The corresponding calculation delay of FFT along azimuth direction is about 51.2ms. So the generation of the modulation signal in T-DIS method can not be done in real-time. In T-DIS method,

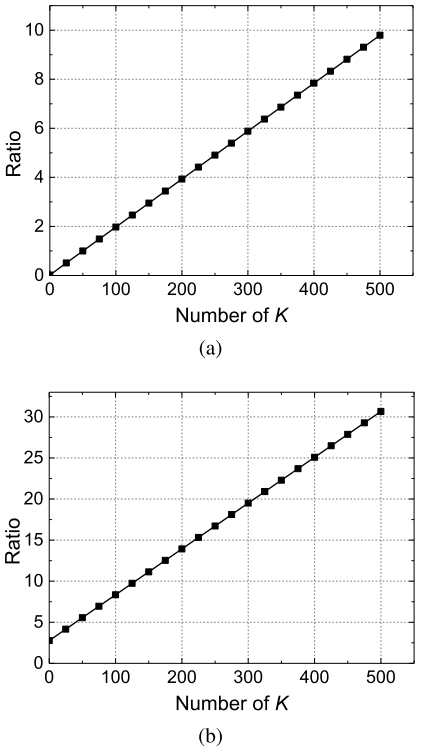

FIGURE 4. The comparison of computation complexity between the proposed method and T-DIS method. (a)Multiplication. (b)Addition.

only $M_s \times N_d$ part of the modulation signal is used to produce the jamming signal. The FFT and the interpolation process the data matrix of which the size is $M_r \times M_d$, the redundant modulation signal is useless and increases the processing time. At each radar pulse, the modulation signal is read out and conducts multiplication to produce the jamming signal. So, T-DIS method needs memory to store the modulation signal.

In our method, each modulation signal is a single-tune signal. After estimating the parameters of radar signal, the jammer generates the modulation signal at the same time when receives and samples the radar signal. Then the phase modulation, the amplitude modulation, and the summation of all the modulation signals are implemented by pipeline technology. The jamming signal is generated by the multiplication of the modulation signal and the intercepted radar signal. These steps take up several periods of FPGA clock, i.e., hundreds of nanoseconds. It can be concluded that the proposed method is real-time during the whole work time of the jammer because the the algorithm need not stop to generate the modulation signal.

In Table. 2, we present the requirement for the computation resource in the two methods. In T-DIS method, the FFT along range direction can be done parallel, while the FFT along azimuth direction must be done one by one. According to the IP core of Xilinx FPGA, the number of multipliers is $9 \times N$ for range FFT, the number of multipliers is 9 for azimuth FFT. The correction signal can be created by DDS, which needs 2 adders for the 2-D correction. The linear interpolation

TABLE 2. The consumption of computation resource in FPGA.

	Procedure	Multiplier	Adder
T-DIS	2-D FFT	$9 \times N + 9$	0
	Correction matrix	2	2
	Linear interpolation	2×2	3×2
	Jamming modulation	1	0
2-D FMDJ	DDS	0	$M + N$
	Doppler modulation	0	K
	Amplitude modulation	K	0
	Summation	0	$K - 1$
	Jamming modulation	1	0

needs 3 additions and 2 multiplications to obtain one result. The computation resource is double for the 2-D interpolation. To produce the jamming signal, one multiplier is required.

In our method, $M + N$ numbers of DDS are used to create the range modulation signal and the Doppler phase. Then the Doppler phase modulation needs K adders and the amplitude modulation requires K multipliers. $K - 1$ adders are used to sum all the modulation signals. The jamming signal created by one multiplier is the same as T-DIS method. Our method demands for more computation resources when compared with T-DIS method. Because the 2-D FFT in T-DIS method works serially, the consumption of computation resource is fewer.

The generation of the modulation signal in T-DIS method relates to the pulses number N_d, which means that the modulation signal should be updated every N_d radar pulses. Considering the computation load, T-DIS method could not produce the jamming signal during the generation of the modulation signal. Further more, we do not know the exact pulses number for an ISAR image. If the T-DIS jamming signal is created based on x radar pulses, while ISAR uses $x + m$ ($x + m$ can be larger or smaller than x) pulses for imaging, the jamming effect of T-DIS method has not been researched. The modulation signal in our method is generated consecutively. No matter how many radar pulses are used for an ISAR image, our algorithm is able to generate the corresponding jamming signal during certain time interval. Since FPGA has thousands of multipliers, the proposed method is able to generate a false target with hundreds of scatterers in real-time.

V. SIMULATIONS

This section is dedicated to the simulation results of the proposed jamming algorithm. The ISAR works at X-band and forms an image by processing of 128 radar pulses. The remaining simulation parameters are presented in Table. 3.

We select an ISAR image of a ship, provided by Sandia National Laboratories [32], as the template of false target. Firstly we build up a template model to simulate the ship. The template contains 350 cells (in range) $\times$ 250 cells (in azimuth) and the resolution is 0.75m (in range) $\times$ 0.5m (in azimuth), as shown in Fig. 5. Then the template is processed

TABLE 3. Simulation parameters.

Parameters	Symbol	Value	Unit
Carrier frequency	f_c	10	GHz
Bandwidth	B	100	MHz
Pulse width	T_p	4	μs
Pulse repetition frequency	PRF	1	kHz
Target distance	r_0	1	km
Target rotation angular velocity	ω	0.1	rad/s

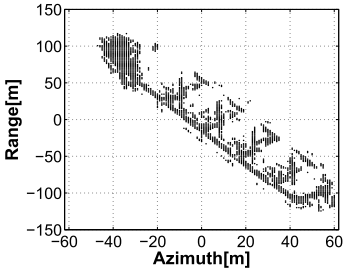

FIGURE 5. The target template of a ship.

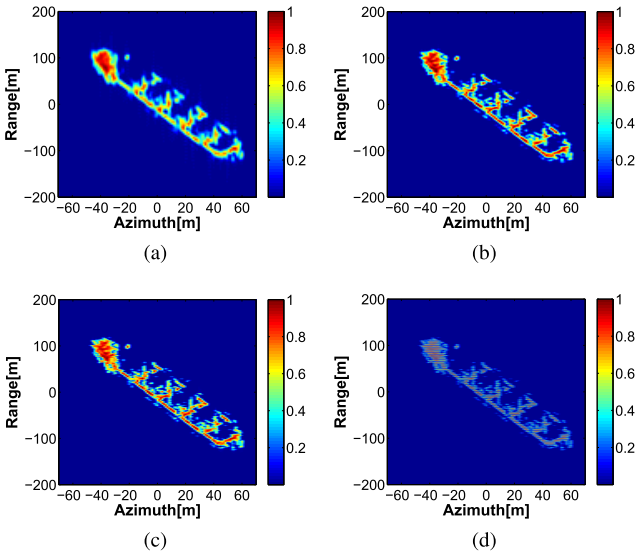

FIGURE 6. The false target jamming effects on ISAR of different range resolutions, $T_p = 4\mu s$. (a)$B = 20$MHz. (b)$B = 50$MHz. (c)$B = 150$MHz. (d)$B = 300$MHz.

to generate the modulation signal according to (5)-(12). The jamming signal is obtained by the multiplication between the radar LFM signal and the modulation signal.

To verify the jamming effect on ISAR of various range resolutions, the jamming algorithm is applied onto the LFM signal of different bandwidths and the results are presented in Fig. 6. We see that the jamming signal is able to generate a false target which is similar to the template on ISAR image. Although the range resolution of the radar signal changes, the range size of the false targets is correct and coincides with the template. The images in Fig. 6(b) and Fig. 6(c) clearly reflect the structure of false target because the image resolution is close to the template's resolution. The false image in Fig. 6(a) is blurred due to the lower radar resolution. When the radar resolution is higher in Fig. 6(d), the scatterers

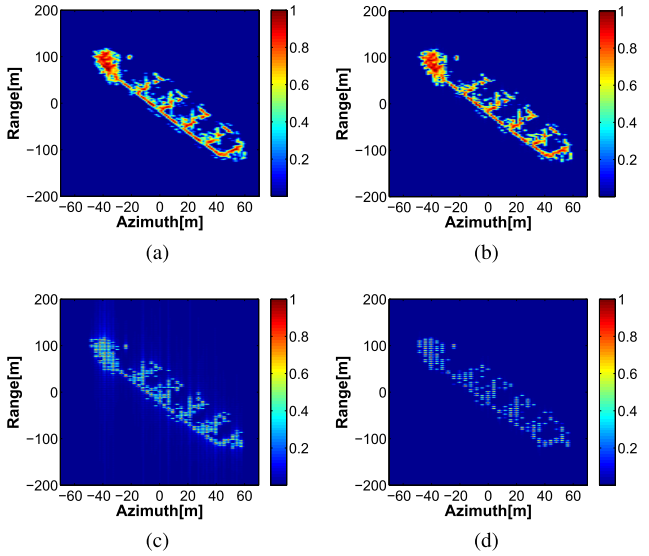

FIGURE 7. The false target images when choosing the template of different resolutions. (a)1m×1m. (b)2m×2m. (c)3m×3m. (d)4m×4m.

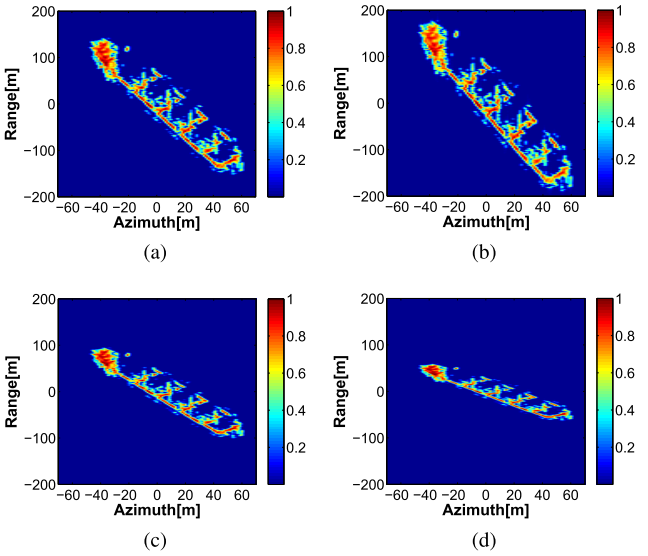

FIGURE 8. The jamming effects caused by the estimating error of chirp rate γ. (a)$\eta_r = +20\%$. (b)$\eta_r = +50\%$. (c)$\eta_r = -20\%$. (d)$\eta_r = -50\%$.

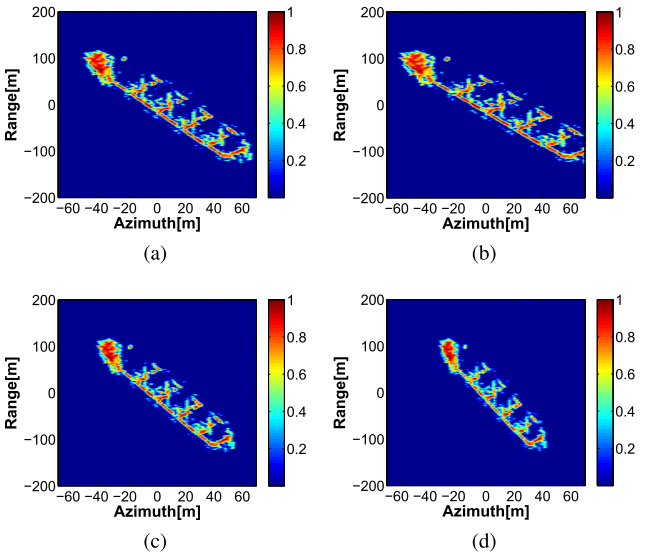

FIGURE 9. The jamming effects when bringing in the estimating error of wavelength λ. (a)$\eta_\lambda = +10\%$. (b)$\eta_\lambda = +30\%$. (c)$\eta_\lambda = -10\%$. (d)$\eta_\lambda = -30\%$.

of the target template are clearly distinguished and ISAR may realize this shortcoming. So the resolution of target template should be as high as possible. But the computation resource also increases as the template becomes more sophisticated.

Next we analyze the influence on ISAR image caused by the resolution of target template. On this occasion, the resolution of ISAR is fixed while the jammer selects the target templates of various resolutions. The resolution of ISAR image is 1.5m in range and 1.2m in azimuth. We see that the false target is vivid if the template resolution is higher or close to the ISAR resolution, shown in Fig. 7(a) and Fig. 7(b). When the resolution of template is lower, the ISAR image of false target lacks of fidelity, shown in Fig. 7(c) and Fig. 7(d).

The previous jamming results are obtained on the assumption that the radar parameters, such as λ and γ, can be estimated by the jammer without error. Now we analyze what the false target looks like if the estimating error exists in γ. According to (22), the range size of false target is determined by γ', which is the foundation to compute the frequency of range modulation signal.

In Fig. 8, we bring in the estimating error η_r in the generation of modulation signal. The simulation results illuminate that η_r only affects the range size of the target and does not change the azimuth size. When $\gamma' > \gamma$, the frequency of the range modulation signal is larger than we need, so the false target becomes longer in range direction. Otherwise, the false target will be shorter, which coincides with the previous analysis. We also see that even the estimating error is quite large, i.e., 50% relative error, the false target can still be imaged.

In the following, we try to explain the influence on the target's azimuth size caused by the errors in λ and ω. According to (25) and (27), the azimuth size of the false target is inversely proportional to the estimating value of λ or ω. The false target is stretched in azimuth direction if the estimating value is smaller than the true value, shown in Fig. 9(a) and Fig. 9(b). In contrast, the azimuth size of the target is narrowed when $\eta_\lambda < 0$, i.e., $\lambda' > \lambda$, shown in Fig. 9(c) and Fig. 9(d).

The jamming effect caused by ω is as same as that of λ, but the reason is different. The error of λ is brought by the jammer and it changes the Doppler frequency of the modulation signal corresponding to each scatterer. That's to say, the azimuth size of the false target contained in the jamming signal is changed by η_λ. The estimating error of ω is caused by ISAR, which results in a display error in the azimuth size of the target on the ISAR image. Similarly, the target image in Fig. 10 is longer when $\eta_\omega > 0$, otherwise is shorter when $\eta_\omega < 0$.

Next the jamming algorithm is applied onto the measured data to verify the performance. The ISAR image of an ocean

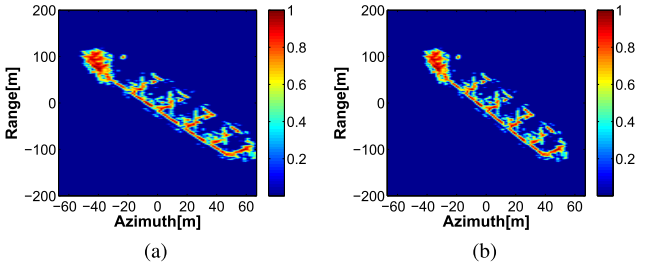

FIGURE 10. The jamming effects influenced by the estimating error of rotating angular velocity ω. (a)$\eta_\omega = +10\%$. (b)$\eta_\omega = -10\%$.

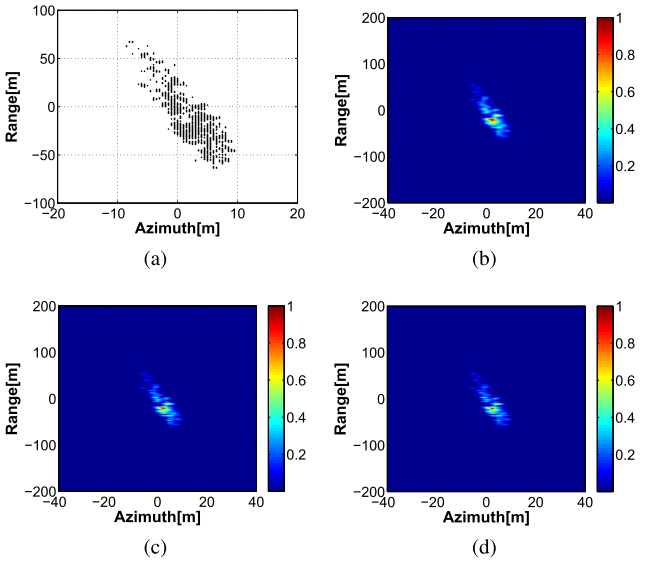

FIGURE 11. The ISAR images of a false liner under various radar resolutions. (a)The template of a liner. (b)$B = 50$MHz. (c)$B = 100$MHz. (d)$B = 200$MHz.

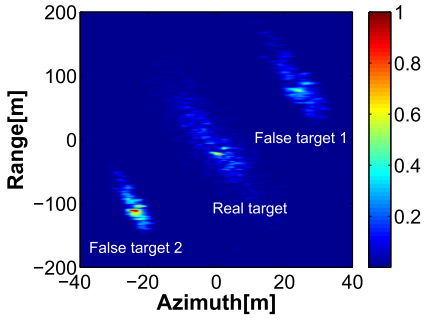

FIGURE 12. The false targets of different sizes, created by adjusting the jamming parameters.

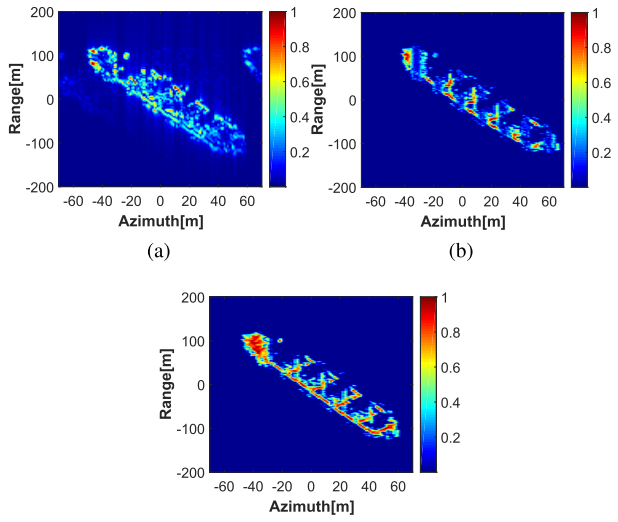

FIGURE 13. The comparison of the false targets created by different methods. (a)T-DIS method. (b)The convolution method. (c)The proposed method.

liner is obtained by an LFM signal of which the bandwidth is 100MHz and the pulse width is 20μs. The false target template, shown in Fig. 11(a), is built up according to the ISAR image. The results in Fig. 11(b)-(d) indicate that the proposed method is capable of generating vivid false targets to ISAR signals of various resolutions. The induced false target, containing the scattering property and proper physical size, is very similar to the real one.

From previous analysis we know that the size of false target is affected by the estimating values of λ and γ. So we can use this property to generate false targets of different sizes. In Fig. 12, the false target 1 (upper-right corner) is enlarged to 1.25 times in dimension, while the false target 2 (lower-left corner) is shrunk to 0.7 times. From (22) and (25) we know that the size of the false target will be different if the jammer uses an inaccurate value of γ and λ to compute the frequency of modulation signal. For example, when computing the frequency of range or azimuth modulation signal, we can amplify or reduce the estimating values of γ or λ to make the modulation frequency bigger or smaller than the demand value. From Fig. 12 we see that two false targets of different sizes are created around the real target. This property provides the jammer with the ability to form false targets of multiple sizes when only one target template is adopted.

At last, the jamming effects of T-DIS method [31], the convolution method [25], and the proposed method are presented in Fig. 13. These three methods are able to form a false target similar to the target's template on ISAR image. The false target in Fig. 13(a) suffers from severe sidebands because the modulation signal in T-DIS method is obtained from the interpolation of 2-D FFT results. Since error exists in the interpolation result, the image of false target smears and the quality of false target decreases. The false target in Fig. 13(b) created by convolution jamming is better than T-DIS method because the high resolution range profile (HRRP) of target is used to generate the jamming signal. The HRRP reflects the target characteristic, including the scattering coefficient, the distribution property of each scatterer, and the shielding of structure, which makes the false target very vivid. However, the computation load of convolution is a heavy burden to the jammer. We think if the FPGA implementation of convolution can be realized parallel and the problem of calculation delay is solved, the convolution method can be an excellent jamming algorithm against ISAR. But now in the situation where the ADC of high sampling frequency is used, the convolution jamming is hard to be implemented. The false target created

by the proposed method is presented in Fig. 13(c). Since no interpolation is used, each scatterer of the false target focuses better than T-DIS method. Considering the computation delay of the three methods, the proposed method is real-time and suitable for engineering implementation.

VI. CONCLUSION

Since ISAR has played an important role in civil or military application domains, the counter-measurements against this powerful weapon attract more and more attentions in recent decades. Most of the proposed deception methods focus on the generation of multiple false targets based on the assumption that the jamming signal is reflected again by the real target or the jammer could receive the target echo, which is really a hard task in the real scene. On most occasions, the jammer is meant to produce the jamming signal by itself. So the jamming algorithm which contains the information of a designed target is very important.

In this paper, we propose a method capable of generating a false target on the ISAR image based on 2-D frequency modulation. The target template is built up according to a real ISAR image, which guarantees the fidelity of false target. If the target template does not consist of many scatterers, the generation of modulation signal is computed in real-time. For a complex target template, the creation of modulation signal can be implemented in the off-line stage since only a few radar parameters are needed. The novelties of this paper include the real-time performance and the ability of generating vivid false targets of different sizes. Besides, the computation load of the method is adequate for the current processor, such as FPGA or DSP. The method can be developed and implemented as a valid deception countermeasure against ISAR due to the excellent real-time performance.

REFERENCES

[1] X. Bai, M. Xing, F. Zhou, and Z. Bao, "High resolution ISAR imaging of targets with rotating parts," *IEEE Trans. Aerosp. Electron. Syst.*, vol. 47, no. 4, pp. 2530–2543, Oct. 2011.

[2] Z. Gu, J. Liu, X.-Y. Pan, X. Ai, B. Liu, and G. Wang, "ISAR imaging with wideband V-FM waveforms via dual-channel CS-D," *IEEE Access*, vol. 5, pp. 18557–18563, 2017.

[3] C. Özdemir, *Inverse Synthetic Aperture Radar Imaging With MATLAB Algorithms*. Hoboken, NJ, USA: Wiley, 2012.

[4] X. Wei, S. Xu, B. Peng, and Z. Liu, "False-target image synthesizer for countering ISAR via inverse dechirping," *J. Syst. Eng. Electron.*, vol. 27, no. 1, pp. 99–110, Feb. 2016.

[5] D. Feng, L. Xu, X. Pan, and X. Wang, "Jamming wideband radar using interrupted-sampling repeater," *IEEE Trans. Aerosp. Electron. Syst.*, vol. 53, no. 3, pp. 1341–1354, Jun. 2017.

[6] L. Xu, D. Feng, Y. Liu, X. Pan, and X. Wang, "A three-stage active cancellation method against synthetic aperture radar," *IEEE Sensors J.*, vol. 15, no. 11, pp. 6173–6178, Nov. 2015.

[7] L. Xu, D. Feng, R. Zhang, and X. Wang, "High-resolution range profile deception method based on phase-switched screen," *IEEE Antennas Wireless Propag. Lett.*, vol. 15, pp. 1665–1668, Jan. 2016.

[8] X.-Y. Pan, W. Wang, and G.-Y. Wang, "Sub-Nyquist sampling jamming against ISAR with CS-based HRRP reconstruction," *IEEE Sensors J.*, vol. 16, no. 6, pp. 1597–1602, Mar. 2016.

[9] L. Xu, D. Feng, and X. Wang, "Improved synthetic aperture radar micro-Doppler jamming method based on phase-switched screen," *IET Radar, Sonar Navigat.*, vol. 10, no. 3, pp. 525–534, Feb. 2016.

[10] W. Wu, K. Cui, H. Lu, T. Meng, and N. Yuan, "A measured rasorber with two absorptive bands," *Radioengineering*, vol. 26, no. 4, pp. 979–983, Dec. 2017.

[11] W. Wu, X. Liu, K. Cui, Y. Ma, and Y. Yuan, "An ultrathin and polarization-insensitive frequency selective surface at Ka-band," *IEEE Antennas Wireless Propag. Lett.*, vol. 17, no. 1, pp. 74–77, Jan. 2018.

[12] J. Xu, B. Bai, C. Dong, and G. Zhao, "A novel passive jamming method against ISAR based on resonance absorption effect of metamaterials," *IEEE Access*, vol. 6, pp. 18142–18148, Mar. 2018.

[13] J. Wang, D. Feng, L. Xu, and W. Hu, "Synthetic aperture radar image modulation using phase-switched screen," *IEEE Antennas Wireless Propag. Lett.*, vol. 17, no. 5, pp. 911–915, May 2018.

[14] J. Wang, D. Feng, Q. Wu, L. Xu, and W. Hu, "Synthetic aperture radar target feature transformation method based on random code phase-switched screen," *IEEE Access*, vol. 6, pp. 41173–41178, Jul. 2018.

[15] L. Xu, D. Feng, and X. Wang, "Matched-filter properties of linear-frequency-modulation radar signal reflected from a phase-switched screen," *IET Radar, SonarNavigat.*, vol. 10, no. 2, pp. 318–324, Feb. 2016.

[16] J. Wang, D. Feng, L. Xu, R. Zhang, and W. Hu, "Synthetic aperture radar target feature modulation using active frequency selective surface," *IEEE Sensors J.*, vol. 19, no. 6, pp. 2113–2125, Mar. 2019.

[17] B. Zhao, L. Huang, J. Li, M. Liu, and J. Wang, "Deceptive SAR jamming based on 1-bit sampling and time-varying thresholds," *IEEE J. Sel. Topics Appl. Earth Observ. Remote Sens.*, vol. 11, no. 3, pp. 939–950, Mar. 2018.

[18] N. Tai, C. Wang, L. Liu, W. Wu, and N. Yuan, "Deceptive jamming method with micro-motion property against ISAR," *Radioengineering*, vol. 26, no. 3, pp. 813–822, Sep. 2017.

[19] X. Shaokun, L. Jihong, F. Yaowen, and L. Xiang, "Deception jamming method for ISAR based on sub-Nyquist sampling technology," in *Proc. IEEE 10th Int. Conf. Signal Process. (ICSP)*, Beijing, China, Oct. 2010, pp. 2023–2026.

[20] X. Pan, J. Liu, J. Chen, Q. Xie, and X. Ai, "Sub-Nyquist sampling jamming against chirp-ISAR with CS-D range compression," *IEEE Sensors J.*, vol. 18, no. 3, pp. 1140–1149, Feb. 2018.

[21] W. Wang, X.-Y. Pan, Y.-C. Liu, D.-J. Feng, and Q.-X. Fu, "Sub-Nyquist sampling jamming against ISAR with compressive sensing," *IEEE Sensors J.*, vol. 14, no. 9, pp. 3131–3136, Sep. 2014.

[22] Z.-Y. Gu, X.-Y. Pan, Q.-X. Fu, W. Wang, and G.-Y. Wang, "Sub-Nyquist sampling jamming against wideband LFM radar with CS-based matched filtering," in *Proc. Prog. Electromagn. Res. Symp. (PIERS)*, Shanghai, China, 2016, pp. 2995–3001.

[23] D. J. Fouts, P. E. Pace, C. Karow, and S. R. T. Ekestorm, "A single-chip false target radar image generator for countering wideband imaging radars," *IEEE J. Solid-State Circuits*, vol. 37, no. 6, pp. 751–759, Jun. 2002.

[24] P. E. Pace, D. J. Fouts, S. Ekestorm, and C. Karow, "Digital false-target image synthesiser for countering ISAR," *IEE Proc.-Radar, Sonar Navigat.*, vol. 149, no. 5, pp. 248–257, Oct. 2002.

[25] Z. Bo, F. Zhou, X. Shi, Q. Wu, and B. Zheng, "Multiple targets deception jamming against ISAR using electromagnetic properties," *IEEE Sensors J.*, vol. 15, no. 4, pp. 2031–2038, Apr. 2015.

[26] J. Chen, X. Pan, L. Xu, and W. Wang, "Deception jamming against ISAR with coupled two-dimensional compressive sensing via sub-Nyquist sampling," *IEEE Access*, vol. 6, pp. 55700–255693, Sep. 2018.

[27] Q. Shi, N. Tai, C. Wang, and N. Yuan, "On deception jamming for countering LFM radar based on periodic 0-π phase modulation," *AEU-Int. J. Electron. Commun.*, vol. 83, pp. 245–252, Jan. 2017.

[28] Q. Shi, C. Wang, J. Huang, and N. Yuan, "Multiple targets deception jamming against ISAR based on periodic 0-π phase modulation," *IEEE Access*, vol. 6, pp. 3539–3548, Jan. 2018.

[29] Q. Shi, J. Huang, T. Xie, C. Wang, and N. Yuan, "An active jamming method against ISAR based on periodic binary phase modulation," *IEEE Sensors J.*, to be published.

[30] X. Pan, W. Wang, D. Feng, Y. Liu, Q. Fu, and G. Wang, "On deception jamming for countering bistatic ISAR based on sub-Nyquist sampling," *IET Radar, Sonar Navigat.*, vol. 8, no. 3, pp. 173–179, Mar. 2014.

[31] L. Xu, D. Feng, X. Pan, Q. Liu, and X. Wang, "An improved digital false-target image synthesizer method for countering inverse synthetic aperture radar," *IEEE Sensors J.*, vol. 15, no. 10, pp. 5870–5877, Oct. 2015.

[32] *Synthetic Aperture Radar (SAR) Imagery, Maritime Search Mode Example of a Ship at Sea*. Accessed: Mar. 17, 2019. [Online]. Available: https://www.sandia.gov/radar/imagery/index.html

[33] Z. De-Ping, X. Shao-Yi, W. Chao, W. Wei-Wei, Z. Chang, and Y. Nai-Chang, "An ultra-high ramp rate arbitrary waveform generator for communication and radar applications," *IEICE Electron. Express*, vol. 12, no. 3, pp. 1–10, Jan. 2015.

NING TAI was born in Shaanxi, China, in 1989. He received the B.S. degree in electronic information engineering from Xidian University, Xi'an, in 2011. He received the M.S. and the Ph.D. degrees in electronic science and technology from National University of Defense Technology, Changsha, in 2013 and 2017, respectively. From 2017 to 2019, he was an Engineer with Luoyang Electronic Equipment Test Center. He is currently an Engineer with State Key Laboratory of Complex Electromagnetic Environment Effects on Electronics and Information System. His research interests include radar signal processing, radar system simulation and countermeasures against ISAR.

HUAN LIN was born Liaoning, China, in 1979. He received the B.S. degree in electronic information engineering from Dalian Maritime University, Dalian, in 2002. He is currently a Senior Engineer with Luoyang Electronic Equipment Test Center. His research interests include radar signal processing and radar engineering.

YONGWEI LU was born in Henan, China, in 1985. He received the B.S. and M.S. degrees in measurement and control technology and instrument from Tianjin University, Tianjin, in 2008 and 2013, respectively. He is currently an Engineer with Luoyang Electronic Equipment Test Center. His research interests include signal processing and simulation in radar system.

HUI HAN was born in Yunnan, China, in 1980. She received the M.S. degree in electronics and communications engineering from National University of Defense Technology, Changsha, in 2010. She is currently an Associate Professor with State Key Laboratory of Complex Electromagnetic Environment Effects on Electronics and Information System. Her research interests include the property and simulation of electromagnetic environment, communication countermeasure.

XIONG XU was born in Fujian, China, in 1985. He received the Ph.D. degree in physical electronics from University of Electronics Science and Technology of China, Chengdu, in 2012. He is currently a Research Associate with State Key Laboratory of Complex Electromagnetic Environment Effects on Electronics and Information System. His research interests include signal processing and machine learning.

YONGHU ZENG was born in Jiangxi, China, in 1972. He received the Ph.D. degree in information and communication engineering from National University of Defense Technology, Changsha, in 2004. He is currently a Professor with State Key Laboratory of Complex Electromagnetic Environment Effects on Electronics and Information System. His research interests include radar signal processing, and simulation and evaluation of electronics and information system.